J|A|C|S ARTICLES

Published on Web 07/21/2009

Unveiling How Stereoelectronic Factors Affect Kinetics and Thermodynamics of Protonation Regiochemistry in [FeFe] Hydrogenase Synthetic Models: A DFT Investigation

Giuseppe Zampella, Piercarlo Fantucci, and Luca De Gioia*

Department of Biotechnology and Biosciences, University of Milano-Bicocca, Piazza della Scienza, 2 20126-Milan, Italy

Received April 6, 2009; E-mail: luca.degioia@unimib.it

Abstract: The DFT investigation of protonation regiochemistry for a series of $[Fe(I)]_2(edt)(PR)_x(CO)_{(6-x)}$ complexes differing for steric and electronic properties of ligands has allowed the disclosure of several key relations between the structure of the complexes and reactivity toward acids, from both a thermodynamics and kinetics perspective. The phosphine/CO ratio strongly affects both the thermodynamics and kinetics of protonation. In particular, with the exception of dppv complexes, in which steric factors become more important, the presence of phosphines, which are better electron donors than CO ligands, leads to lower reaction barriers. The presence of bulky phosphine ligands, which severely hinder the accessibility to the Fe−Fe bond, is a crucial factor responsible for kinetic preference of terminal- versus μ-protonation in symmetric complexes. The investigation of asymmetric models allowed us to rationalize why protonation takes place preferentially on the less electron-rich iron atom, i. e., the iron atom coordinated by the largest number of CO ligands. Importantly, the presence of *at least one* electron-donor ligand on the protonating Fe atom is fundamental to allow facile terminal protonation, suggesting that one of the reasons for the presence of CN^- ligands in the enzyme might be related to the facile formation of catalytically relevant terminally protonated species. Finally, it was found that poorly reacting μ-H Fe(II)Fe(II) species are always thermodynamically more stable than corresponding terminal-hydride forms, indicating that one of the main challenges for the development of efficient synthetic catalysts inspired to the [FeFe] hydrogenase active site will be the design of complexes that undergo terminal protonation but cannot interconvert to the corresponding μ-H forms.

Introduction

Hydrogenases are enzymes that catalyze proton reduction and have been the subject of intensive studies both for their biological relevance and for their potential utilization as efficient catalysts to produce dihydrogen for industrial applications.[1−19] In particular, [FeFe] hydrogenases, which are characterized by a peculiar Fe_6S_6 cluster (composed by a Fe_4S_4 and a Fe_2S_2 unit; see Scheme 1) in their active site,[20−23] have been extensively investigated. Proton reduction in the active site of the enzyme is thought to take place on the Fe_2S_2 subunit (referred to as the $[2Fe]_H$ cluster), and this observation has stimulated the synthesis of several diiron complexes resembling key structural features of the $[2Fe]_H$ cluster, having as the main target the production of synthetic catalysts.[24−37] However, very few efficient catalysts for proton reduction have been obtained so far. One of the reasons for the very different catalytic activity of the enzyme when compared to synthetic catalysts is thought to stem from the different regiochemistry of proton binding to Fe(I)Fe(I) species.

In fact, available experimental and theoretical data suggest that, in the enzyme, protons bind in a terminal fashion to the distal iron center (Fe_d; see Scheme 1) of the $[2Fe]_H$ cluster, whereas proton binding to Fe(I)Fe(I) organometallic complexes eventually leads to μ-H species, which usually are not very

(1) Albracht, S. P. *Biochim. Biophys. Acta* **1994**, *1188*, 167–204.
(2) Adams, M. W.; Mortenson, L. E.; Chen, J. S. *Biochim. Biophys. Acta* **1980**, *594*, 105–76.
(3) Cammack, R.; Fernandez, V. M.; Schneider, K. *Biochimie* **1986**, *68*, 85–91.
(4) Cammack, R. *Nature* **1999**, *397*, 214–5.
(5) Cammack, R. *Biochem. Soc. Trans.* **2005**, *33*, 1–2.
(6) Nicolet, Y.; Fontecilla-Camps, J. C. *Actual. Chim.* **2001**, 34–37.
(7) Nicolet, Y.; Cavazza, C.; Fontecilla-Camps, J. C. *J. Inorg. Biochem.* **2002**, *91*, 1–8.
(8) Volbeda, A.; Fontecilla-Camps, J. C. *Dalton Trans.* **2003**, 4030–4038.
(9) Armstrong, F. A.; Fontecilla-Camps, J. C. *Science* **2008**, *321*, 498–499.
(10) Peters, G. A.; Evans, W. R.; Toia, R. E. *Plant Physiol.* **1976**, *58*, 119–126.
(11) Nicolet, Y.; Lemon, B. J.; Fontecilla-Camps, J. C.; Peters, J. W. *Trends Biochem. Sci.* **2000**, *25*, 138–43.
(12) Peters, J. W.; Lemon, B. J.; Shankarling, G. *Abstr. Pap. Am. Chem. Soc.* **2002**, *224*, U645–U645.
(13) Voordouw, G.; Armstrong, S. M.; Reimer, M. F.; Fouts, B.; Telang, A. J.; Shen, Y.; Gevertz, D. *Appl. Environ. Microbiol.* **1996**, *62*, 1623–1629.
(14) Leger, C.; Jones, A. K.; Roseboom, W.; Albracht, S. P. J.; Armstrong, F. A. *Biochemistry* **2002**, *41*, 15736–15746.
(15) Lamle, S. E.; Vincent, K. A.; Halliwell, L. M.; Albracht, S. P. J.; Armstrong, F. A. *Dalton Trans.* **2003**, 4152–4157.
(16) Armstrong, F. A. *Curr. Opin. Chem. Biol.* **2004**, *8*, 133–140.
(17) Vincent, K. A.; Armstrong, F. A. *Inorg. Chem.* **2005**, *44*, 798–809.
(18) Vincent, K. A.; Li, X.; Blanford, C. F.; Belsey, N. A.; Weiner, J. H.; Armstrong, F. A. *Nat. Chem. Biol.* **2007**, *3*, 760–761.
(19) Kubas, G. J. *Chem. Rev.* **2007**, *107*, 4152–205.

Scheme 1. Most Plausible Structure of the Protonated [FeFe] Hydrogenase Cofactor[a]

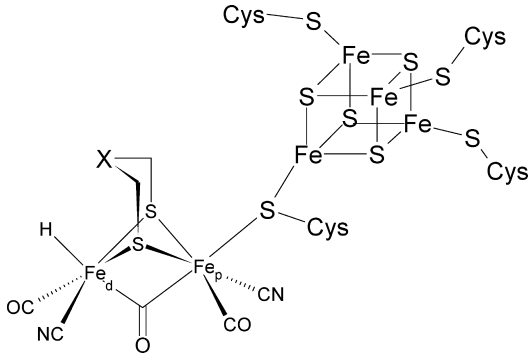

[a] Fe_p and Fe_d stand for "proximal" and "distal" iron, respectively, relative to the Fe_4S_4 cluster. Both experimental and theoretical evidences suggest terminal binding of H^+ to Fe_d.

reactive in the H_2 formation reaction.[38−42] Indeed, in a few cases it was possible to unambiguously characterize biomimetic FeFe synthetic complexes featuring a terminal hydride. However, these complexes are only stable at extremely low temperatures and spontaneously rearrange to the corresponding μ-H species.[35,43−47] Very recently, terminal hydride species have been also postulated as transient intermediates formed during electrochemical proton reduction mediated by synthetic models of [FeFe] hydrogenases.[48]

In light of the above observations, it is particularly relevant to understand which factors affect protonation regiochemistry, from both a thermodynamic and kinetic perspective. To contribute to shedding light on such an issue, we have carried out a DFT investigation of the reactivity toward H^+ of the organometallic complex (dppv)(CO)Fe(edt)Fe(PMe_3)$(CO)_2$ (**1**), as well as of its congeners $(CO)_3$Fe(edt)Fe$(CO)_3$ (**2**), (dppv)(CO)-Fe(edt)Fe$(CO)_3$ (**3**), $(PH_3)_2$(CO)Fe(edt)Fe$(CO)_3$ (**4**), $(PMe_3)_2$-(CO)Fe(edt)(CO)$(PMe_3)_2$ (**5**), (dppv)(CO)Fe(pdt)Fe(dppv)(CO) (**6**), $(PH_3)_2$(CO)Fe(edt)(CO)$(PH_3)_2$ (**7**), and $(PH_3)_3$Fe(edt)-$(PH_3)(CO)_2$ (**7a**). In this set of complexes, dppv stands for $Ph_2PCHCHPPh_2$ and edt/pdt for ethylene/propylenedithiolate. The choice of this set of complexes is motivated by their similarity to the $[2Fe]_H$ cluster in terms of stereoelectronic properties (such as in **1**; see Scheme 2) and by the observation that most of them have actually been synthesized (**1**, **2**, **5**, and **6**). In addition, the structure of the terminal-H form of **5** has been solved by X-ray diffraction,[49] and a terminal hydride isomer of a complex very closely resembling **3** was characterized by ^{1}H NMR at low temperature.[43] Even though separating electronic from steric effects is an intrinsically impossible task, the set featuring PH_3 ligands (**4**, **7**, **7a**) has been taken into account to explore the effect of decreasing the steric hindrance characterizing some experimentally used donor ligands (PMe_3, dppv).

The main goal of our investigation was isolating as much as possible the effects of the (i) number of P ligands; (ii) steric hindrance (mainly related to the size of P ligands); and (iii) electronic asymmetry (mainly related to the distribution of P ligands onto Fe atoms), on the kinetics and thermodynamics of protonation.

All investigated complexes except one (**6**) are characterized by the presence of edt as the chelating ligand. This choice stems from the observation that bulkier dithiolate ligands (such as pdt) can lead to larger numbers of isomers,[50] complicating the computational analysis. The only investigated complex featuring pdt is **6**, which corresponds to a very recently reported species capable of undergoing terminal protonation.[47]

Methods

Density functional theory (DFT) calculations have been carried out with the TURBOMOLE 5.7 suite.[51] Geometry optimizations and transition state searches have been carried out using the pure functional B-P86,[52,53] in conjunction with a valence triple-ζ basis

(20) Peters, J. W.; Lanzilotta, W. N.; Lemon, B. J.; Seefeldt, L. C. *Science* **1998**, *282*, 1853–8.
(21) Peters, J. W.; Lanzilotta, W. N.; Lemon, B. J.; Seefeldt, L. C. *J. Inorg. Biochem.* **1999**, *74*, 44–44.
(22) Nicolet, Y.; Piras, C.; Legrand, P.; Hatchikian, C. E.; Fontecilla-Camps, J. C. *Structure* **1999**, *7*, 13–23.
(23) Nicolet, Y.; de Lacey, A. L.; Vernede, X.; Fernandez, V. M.; Hatchikian, E. C.; Fontecilla-Camps, J. C. *J. Am. Chem. Soc.* **2001**, *123*, 1596–601.
(24) Gloaguen, F.; Rauchfuss, T. B. *Chem. Soc. Rev.* **2009**, *38*, 100–108.
(25) Rauchfuss, T. B. *Science* **2007**, *316*, 553–554.
(26) Mealli, C.; Rauchfuss, T. B. *Angew. Chem., Int. Ed.* **2007**, *46*, 8942–4.
(27) Singleton, M. L.; Bhuvanesh, N.; Reibenspies, J. H.; Darensbourg, M. Y. *Angew. Chem., Int. Ed.* **2008**, *47*, 9492–9495.
(28) Tye, J. W.; Hall, M. B.; Darensbourg, M. Y. *Proc. Natl. Acad. Sci. U.S.A.* **2005**, *102*, 16911–16912.
(29) Georgakaki, I. P.; Thomson, L. M.; Lyon, E. J.; Hall, M. B.; Darensbourg, M. Y. *Coord. Chem. Rev.* **2005**, *249*, 1133–1133.
(30) Tard, C.; Liu, X.; Ibrahim, S. K.; Bruschi, M.; De Gioia, L.; Davies, S.; Yang, X.; Wang, L.-S.; Pickett, C. J. *Nature* **2005**, *433*, 610–613.
(31) Ridley, A. R.; Stewart, A. I.; Adamczyk, K.; Ghosh, H. N.; Kerkeni, B.; Guo, Z. X.; Nibbering, E. T. J.; Pickett, C. J.; Hunt, N. T. *Inorg. Chem.* **2008**, *47*, 7453–7455.
(32) Liu, X. M.; Ibrahim, S. K.; Tard, C.; Pickett, C. J. *Coord. Chem. Rev.* **2005**, *249*, 1641–1652.
(33) Evans, D. J.; Pickett, C. J. *Chem. Soc. Rev.* **2003**, *32*, 268–275.
(34) Ezzaher, S.; Capon, J. F.; Gloaguen, F.; Petillon, F. Y.; Schollhammer, P.; Talarmin, J.; Kervarec, N. *Inorg. Chem.* **2009**, *48*, 2–4.
(35) Ezzaher, S.; Capon, J. F.; Gloaguen, F.; Kervarec, N.; Petillon, F. Y.; Pichon, R.; Schollhammer, P.; Talarmin, J. *C. R. Chim.* **2008**, *11*, 906–914.
(36) Roy, L. E.; Batista, E. R.; Hay, P. J. *Inorg. Chem.* **2008**, *47*, 9228–9237.
(37) Liu, T. B.; Darensbourg, M. Y. *J. Am. Chem. Soc.* **2007**, *129*, 7008–9.
(38) Nehring, J. L.; Heinekey, D. M. *Inorg. Chem.* **2003**, *42*, 4288–4292.
(39) Gloaguen, F.; Lawrence, J. D.; Rauchfuss, T. B.; Benard, M.; Rohmer, M. M. *Inorg. Chem.* **2002**, *41*, 6573–82.
(40) Gloaguen, F.; Lawrence, J. D.; Rauchfuss, T. B. *J. Am. Chem. Soc.* **2001**, *123*, 9476–7.
(41) Zhao, X.; Georgakaki, I. P.; Miller, M. L.; Yarbrough, J. C.; Darensbourg, M. Y. *J. Am. Chem. Soc.* **2001**, *123*, 9710–1.
(42) Zhao, X.; Georgakaki, I. P.; Miller, M. L.; Mejia-Rodriguez, R.; Chiang, C. Y.; Darensbourg, M. Y. *Inorg. Chem.* **2002**, *41*, 3917–28.
(43) Ezzaher, S.; Capon, J. F.; Gloaguen, F.; Petillon, F. Y.; Schollhammer, P.; Talarmin, J.; Pichon, R.; Kervarec, N. *Inorg. Chem.* **2007**, *46*, 3426–8.
(44) Morvan, D.; Capon, J. F.; Gloaguen, F.; Le Goff, A.; Marchivie, M.; Michaud, F.; Schollhammer, P.; Talarmin, J.; Yaouanc, J. J.; Pichon, R.; Kervarec, N. *Organometallics* **2007**, *26*, 2042–2052.
(45) Orain, P. Y.; Capon, J. F.; Kervarec, N.; Gloaguen, F.; Petillon, F.; Pichon, R.; Schollhammer, P.; Talarmin, J. *Dalton Trans.* **2007**, 3754–3756.
(46) Adam, F. I.; Hogarth, G.; Kabir, S. E.; Richards, D. *C. R. Chim.* **2008**, *11*, 890–905.
(47) Barton, B. E.; Rauchfuss, T. B. *Inorg. Chem.* **2008**, *47*, 2261–2263.
(48) Cheah, M. H.; Tard, C.; Borg, S. J.; Liu, X. M.; Ibrahim, S. K.; Pickett, C. J.; Best, S. P. *J. Am. Chem. Soc.* **2007**, *129*, 11085–11092.
(49) van der Vlugt, J. I.; Rauchfuss, T. B.; Whaley, C. M.; Wilson, S. R. *J. Am. Chem. Soc.* **2005**, *127*, 16012–3.
(50) Justice, A. K.; Zampella, G.; De Gioia, L.; Rauchfuss, T. B. *Chem. Commun.* **2007**, 2019–2021.
(51) Ahlrichs, R.; Bar, M.; Haser, M.; Horn, H.; Kolmel, C. *Chem. Phys. Lett.* **1989**, *162*, 165–169.
(52) Becke, A. D. *Phys. Rev. A: At., Mol., Opt. Phys.* **1988**, *38*, 3098–3100.
(53) Perdew, J. P. *Phys. Rev. B: Condens. Matter* **1986**, *33*, 8822–8824.

Scheme 2. Stereoelectronic Similarity between the Organometallic Complex **1** and the $[2Fe]_H$ Cluster

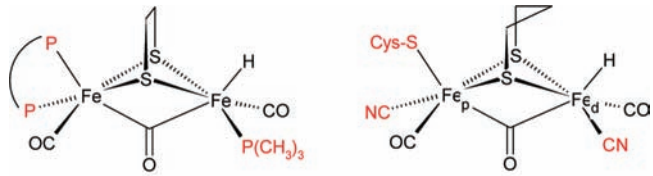

1

set with polarization on all atoms, a level of theory which has been shown to be suited to reliably investigating [FeFe] hydrogenase models.[54−56]

Stationary points of the energy hypersurface have been located by means of energy gradient techniques, and a full vibrational analysis has been carried out to further characterize each stationary point.

The optimization of transition state structures has been carried out according to a procedure based on a pseudo Newton−Raphson method. Initially, geometry optimization of a guessed transition state structure is carried out constraining the distance corresponding to the reaction coordinate. Vibrational analysis at the B-P86/TZVP level of the constrained minimum energy structures is then carried out, and if one negative eigenmode corresponding to the reaction coordinate is found, the curvature determined at such a point is used as the starting point in the transition state search. The location of the transition state structure is carried out using an eigenvector-following search: the eigenvectors in the Hessian are sorted in ascending order, the first one being that associated to the negative eigenvalue. After the first step, however, the search is performed by choosing the critical eigenvector with a maximum overlap criterion, which is based on the dot product with the eigenvector followed at the previous step.

Gibbs free energy (G) values have been obtained from the electronic SCF energy considering three contributions to the total partition function (Q), namely $q_{translational}$, $q_{rotational}$, $q_{vibrational}$, under the assumption that Q may be written as the product of such terms. To evaluate enthalpy and entropy contributions, the values of temperature and pressure have been set to 273.15 K and 1 bar, respectively, to reproduce as closely as possible experimental conditions. Rotations have been treated classically, and vibrational modes described according to the harmonic approximation.

All Gibbs free energy differences have been computed by correcting gas phase data with the inclusion of an implicit treatment of solvent effect (COSMO).[57] The ε value has been set to 37.5 (corresponding to acetonitrile).

In light of available experimental data and considering the chemical nature of the ligands, only low-spin species have been investigated.

In the following, when discussing synthetic models, Fe_p and Fe_d always correspond to the iron atoms coordinated by the largest and fewest number of phosphine ligands, respectively.

Results

We have initially investigated the protonation of [(dppv)-(CO)Fe(edt)Fe(PMe_3)$(CO)_2$] (**1**), which quite closely mimics the most peculiar stereoelectronic features of the $[2Fe]_H$ cluster (Scheme 2) and has been the subject of recent experimental investigations.[58] Triflic acid (CF_3SO_3H) was chosen as the prototypical acid moiety because it is often used experimentally for the protonation of dinuclear complexes resembling the $[2Fe]_H$ cluster of [FeFe] hydrogenases.[59−62]

DFT optimization of **1**, starting from different initial ligand arrangements, led to the characterization of the species **1a** as the most stable isomer (Figure 1). In **1a** the P atoms of the dppv ligand (which are both coordinated to the Fe ion which hereafter is referred to as Fe_p) assume apical and basal positions, while the PMe_3 ligand coordinated to the distal (relative to dppv) iron ion (hereafter referred to as Fe_d) occupies a basal position. Note that a [(dppv)(CO)Fe(edt)Fe(PMe_3)$(CO)_2$] isomer featuring the apical PMe_3 position (**1b**; Figure 1), as observed in the X-ray structure of the corresponding synthetic complex,[58] is computed to be only 0.4 kcal/mol higher in energy than **1a**, suggesting that **1a** and **1b** might coexist in solution. Analysis of bond distances and angles revealed a very good agreement between DFT and X-ray structures (differences below 0.06 Å and 6.0°; see Supporting Information).

Sampling of the potential energy surface (carried out starting optimizations from different initial geometries) led also to the

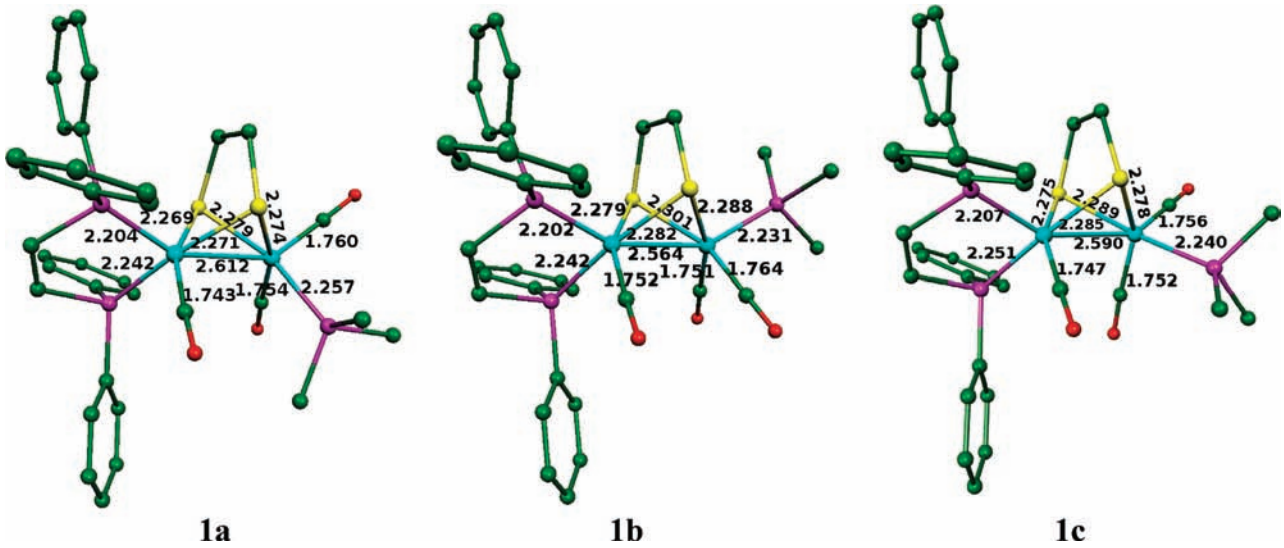

1a **1b** **1c**

Figure 1. Structures of the thermodynamically most stable **1** isomers computed by DFT. Interatomic distances in Å.

Scheme 3. Reaction Pathways for the Reaction **1** + CF_3SO_3H Leading to μ- or Terminal-Protonated Species

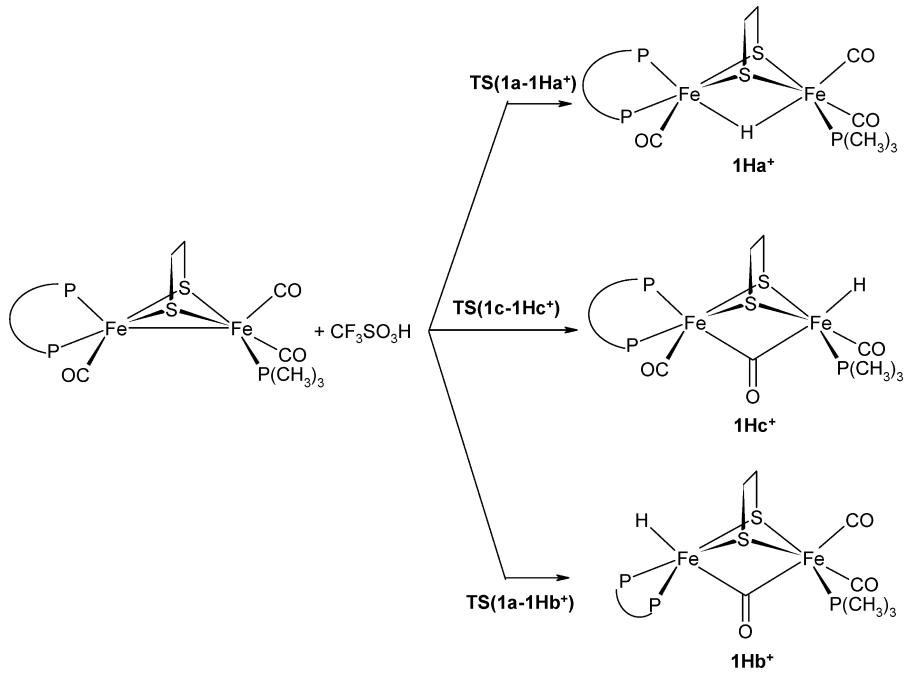

characterization of another almost isoenergetic isomer of **1** (**1c**, Figure 1, ΔG relative to **1a** = 0.6 kcal mol^{-1}), in which the coordination environment of Fe_p is unmodified relative to **1a**, whereas one CO group coordinated to Fe_d approaches the Fe_p atom, moving to a semibridging position. In **1c** the Fe_d ligands are best described as having a trigonal bipyramidal geometry.

Protonation of **1** can take place at the Fe−Fe bond or at the terminal position on Fe_p or Fe_d, leading to μ-H (**1Ha**$^+$) or terminal-H (**1Hb**$^+$ and **1Hc**$^+$) isomers, respectively (Scheme 3). Note that the reaction path leading to **1Hc**$^+$ (i.e., terminal protonation at Fe_d) goes through the intermediate species **1c**, in which a CO group coordinated to Fe_d moves to a semibridging position (Figure 2).

Protonation of **1a** along the Fe−Fe bond takes place going through a transition state, **TS(1a-1Ha**$^+$**)**, in which both Fe ions have a square pyramidal geometry and the proton moving from CF_3SO_3H to the diiron bond is closer to the Fe_p atom (Fe_p−H = 2.042 Å; Figure 2). The energy barrier to **TS(1a-1Ha**$^+$**)** is 15.2 kcal/mol.

The transition state along the **1c** + CF_3SO_3H → **1Hc**$^+$ + $CF_3SO_3^-$ path, **TS(1c-1Hc**$^+$**)**, is characterized by further movement of a CO group coordinated to Fe_d to the semibridging position and concomitant movement of the other CO group coordinated to Fe_d from the apical to basal position. In other words, terminal protonation implies an ∼120° "rotation" of two ligands of the $Fe(L)_3$ moiety where protonation takes place. The energy barrier to **TS(1c-1Hc**$^+$**)** is computed to be very low (5.8 kcal/mol; see also Scheme 4). On the other hand, the reaction pathway to **1Hb**$^+$ (i.e., protonation of the iron atom coordinated by dppv) is characterized by a high reaction barrier (21.3 kcal/mol). The large differences in reaction barriers computed for terminal protonation at Fe_d or Fe_p are due to electronic and steric factors. In fact, Fe_p is electron richer than Fe_d (due to the different number of coordinated phosphine groups), and therefore the rotation of the $Fe_d(CO)_2(PMe_3)$ moiety, which brings a π-acceptor CO group in the semibridging position, is favored relative to the rotation of the Fe(CO)(dppv) moiety, as clearly evident also from the very different Fe−μ(CO) distances in **TS(1c-1Hc**$^+$**)** (Figure 2) and **TS(1b-1Hb**$^+$**)** (Figure 3). In addition, the Fe_p atom is sterically less accessible than Fe_d, due to the bulkiness of the dppv ligand.

In summary, the energy barrier to overcome to form the μ-H species **1Ha**$^+$ is ∼8.8 kcal/mol higher than the corresponding one leading to the more easily formed terminal-H species **1Hc**$^+$ (Scheme 4).

A comparison between **TS(1c-1Hc**$^+$**)** and **TS(1a-1Ha**$^+$**)** reveals that steric factors are important to explain the different barrier heights leading to terminal- and μ-hydride species. In fact, in **TS(1c-1Hc**$^+$**)** the approaching CF_3SO_3H does not experience significant steric interactions with the ligands forming the Fe_d coordination environment, whereas in **TS(1a-1Ha**$^+$**)** the oxygen atoms of CF_3SO_3H clash against the phenyl groups of dppv and the methyl groups of PMe_3 (Figure 4).

The more pronounced steric clashes in **TS(1a-1Ha**$^+$**)**, relative to **TS(1c-1Hc**$^+$**)**, are also highlighted by the Fe−H distance, which in **TS(1a-1Ha**$^+$**)** is larger by more than 0.2 Å due to the hindered accessibility of the Fe−Fe bond (Figure 2). Since **1a** and **1b** isomers are very close in energy, and in the latter the Fe−Fe bond is sterically less hindered, we have also computed the energy barrier corresponding to protonation of the Fe−Fe bond in **1b**, finding that it is lower than that for **1a** by only 2.6 kcal/mol. It is also worth noting that the Fe−Fe bond in **1** is so buried (Supporting Information; Figure 1S) that similar values of reaction barriers are computed also when acids less sterically demanding than CF_3SO_3H are taken into account (data not shown).

These results show how both steric and electronic factors are fundamental to understand why the kinetically controlled product of protonation of the diiron complex **1** corresponds to the terminal-H species **1Hc**$^+$ and complement previous studies in which the role of electronic and steric factors on the properties of [FeFe] hydrogenase synthetic models was highlighted.[63−65]

Since it has been extensively reported that terminally protonated forms spontaneously isomerize to μ-protonated species,[47,49,66] it is interesting to evaluate the relative thermodynamic stability of the different protonated isomers. Protonation

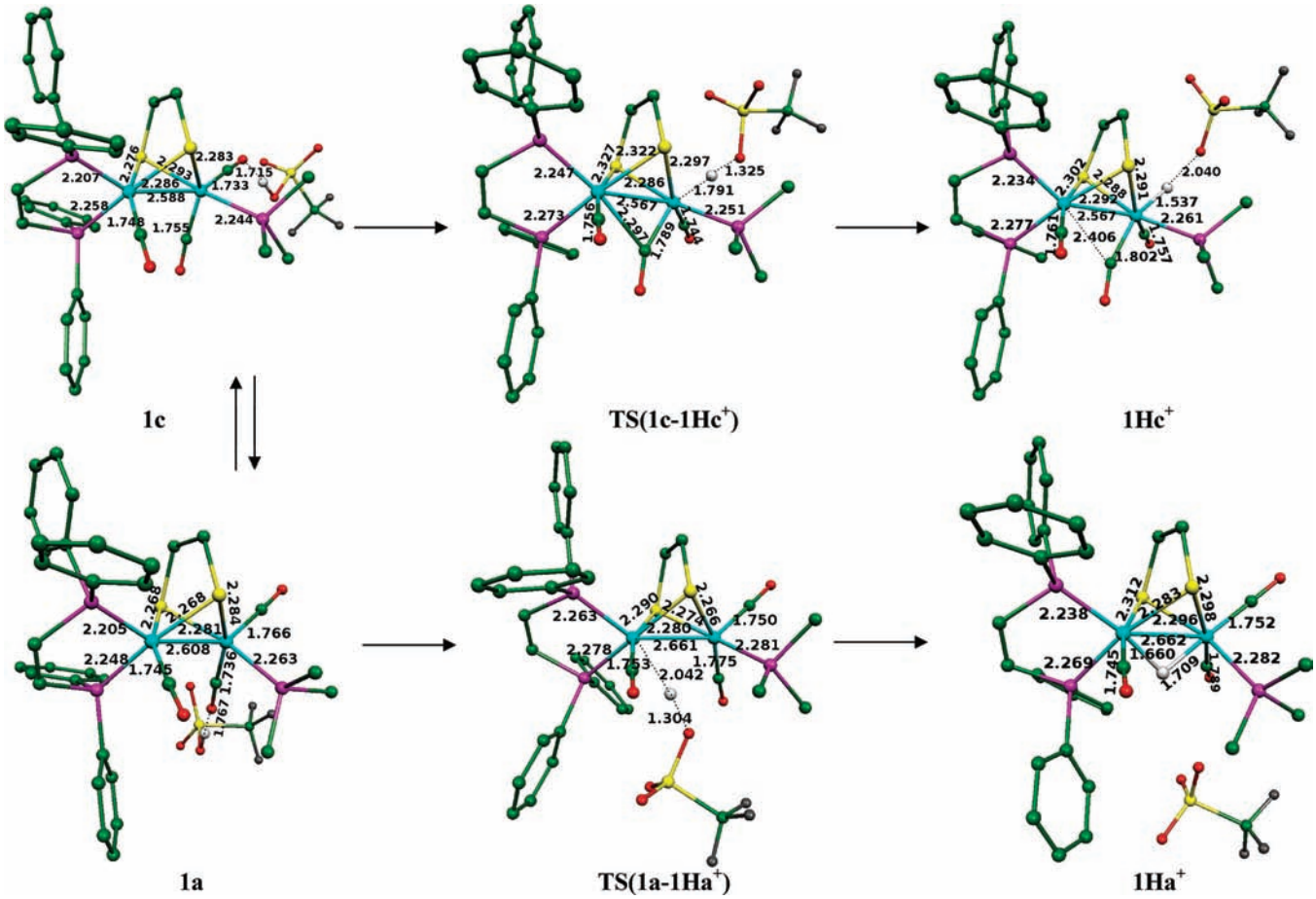

Figure 2. Protonation mechanism of **1a** and **1c**, as characterized by DFT calculations. Atoms are colored according to the following rule. Carbon, green; hydrogen, white; sulfur, yellow; iron, light blue; phosphorus, purple; oxygen, red.

Scheme 4. Free Energy Profile Corresponding to Protonation of (dppv)(CO)Fe(edt)Fe(PMe$_3$)(CO)$_2$ (**1**) at the Fe−Fe Bond (**1a**→**1Ha**$^+$) or at Terminal Position (**1a**→**1Hc**$^+$)

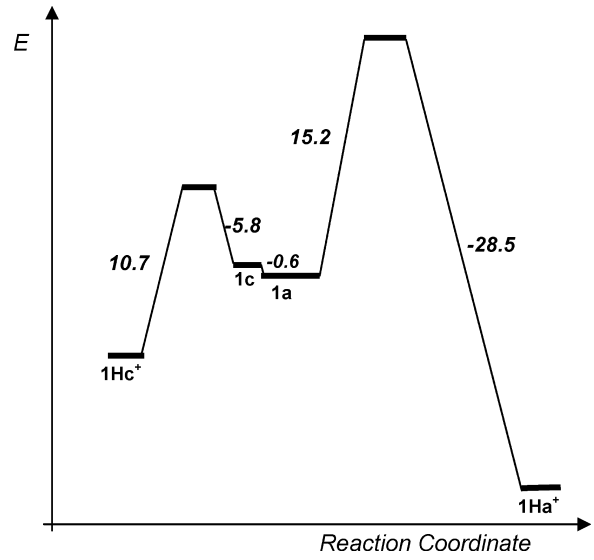

of **1** by CF_3SO_3H at the Fe−Fe bond or at terminal positions corresponds to exoergonic reactions ($\Delta G = -13.3$ and -4.9 kcal/mol, respectively). In particular, it turned out that terminal protonation at Fe_d is slightly favored relative to protonation at Fe_p (by 1.6 kcal/mol). Moreover, as observed in all organometallic $[2Fe]_H$ model complexes investigated so far by DFT, protonation of **1** at the Fe−Fe bond is significantly more favored (by −9.0 kcal/mol) than formation of terminal-H species.

With the aim of generalizing the results obtained studying complex **1**, and further evaluating the effects of electronic and steric properties, as well as the asymmetric disposition of phosphine ligands, the study of the reactivity toward acid species was then extended to the set of complexes:

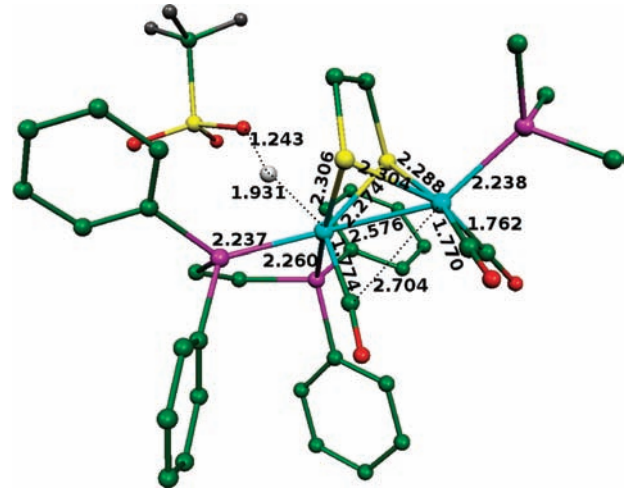

Figure 3. Structure of the transition state **TS(1b-1Hb**$^+$**)**, leading to terminal protonation of the proximal iron atom. Atoms are colored according to the following rule. Carbon, green; hydrogen, white; sulfur, yellow; iron, light blue; phosphorus, purple; oxygen, red.

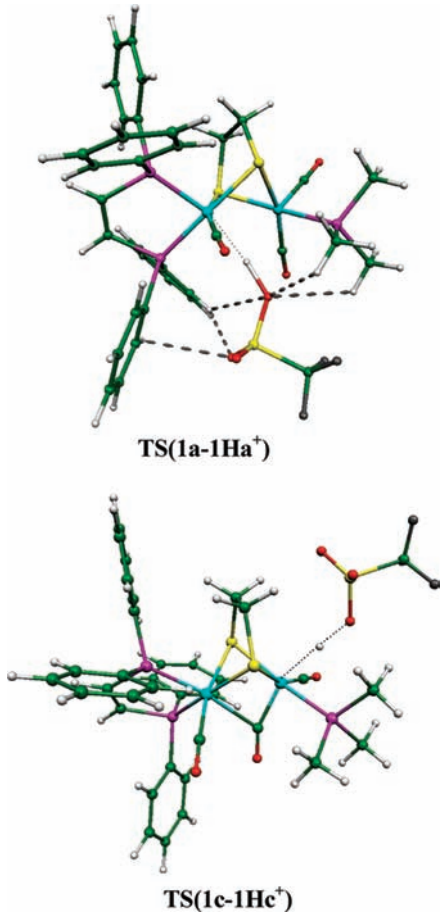

Figure 4. Ball and stick representation of the transition states for proton transfer to the Fe−Fe bond **TS(1a-1Ha$^+$)** and to Fe_d **TS(1c-1Hc$^+$)**. A thin dotted line highlights the reaction coordinate, while bold dashed lines show repulsive interactions. Atoms are colored according to the following rule. Carbon: green, hydrogen: white, sulfur: yellow, iron: light blue, phosphorus: purple, oxygen: red.

- $(CO)_3Fe(edt)Fe(CO)_3$ (**2**); where no phosphine ligands are present.
- (dppv)(CO)Fe(edt)Fe(CO)$_3$ (**3**); $(PH_3)_2(CO)_2Fe(edt)Fe(CO)_3$ (**4**); where two phosphine ligands are present.
- $(PMe_3)_2(CO)Fe(edt)(CO)(PMe_3)_2$ (**5**), (dppv)(CO)Fe(pdt)-(CO)(dppv) (**6**), $(PH_3)_2(CO)Fe(edt)(CO)(PH_3)_2$ (**7**), $(PH_3)_3Fe(edt)-(CO)_2(PH_3)$ (**7a**); where four phosphine ligands are present.

Computed kinetics and thermodynamics data for the reaction of this set of complexes with CF_3SO_3H (corresponding to protonation at μ and terminal position on Fe_d) are collected in Table 1.

The DFT study of the reactivity of **2** reveals that μ-protonation is strongly endoergonic (11.3 kcal/mol), as expected due to the presence of only π-acceptor CO ligands, in agreement with experimental results showing that hexacarbonyl derivatives cannot be protonated even by strong acids. Indeed, protonation of hexacarbonyl derivatives takes place after monoelectron reduction, also in this case leading to μ-hydride species that are thermodynamically more stable than the corresponding terminal-hydride forms.[54]

The reaction energy barrier for the protonation of **2** is only 1.9 kcal/mol higher than that computed for protonation of **1**. Notably, the product of terminal protonation of **2** does not correspond to an energy minimum structure and evolves back to reactants.

Table 1. Kinetic and Thermodynamic Data for the Protonation at Fe−Fe Bond or Terminal (Fe_d) Position, as Obtained by DFT Calculations for the Set of Investigated Complexes[a]

	μ-protonation		terminal-protonation on Fe_d	
	ΔG	$\Delta G^{\ddagger}$	ΔG	$\Delta G^{\ddagger}$
[(dppv)(CO)Fe(edt)Fe(PMe$_3$)(CO)$_2$] (**1**)	−13.3	15.2	−4.9	6.4
$(CO)_3Fe(edt)Fe(CO)_3$ (**2**)	11.3	17.1	−[b]	−
(dppv)(CO)Fe(edt)Fe(CO)$_3$ (**3**)	−1.0	18.3	9.2	−
$(PH_3)_2(CO)Fe(edt)Fe(CO)_3$ (**4**)	−2.3	18.9	−[b]	−
$(PMe_3)_2(CO)Fe(edt)(CO)(PMe_3)_2$ (**5**)	−26.3	7.9	−23.5	5.6
(dppv)(CO)Fe(pdt)Fe(dppv)(CO) (**6**)	−19.5	19.6	−15.7	16.6
$(PH_3)_2(CO)Fe(edt)(CO)(PH_3)_2$ (**7**)	−13.3	8.1	−3.4	10.9
$(PH_3)_3Fe(edt)(PH_3)(CO)_2$ (**7a**)	−19.4	6.0	−8.1	0.0

[a] Energy values (kcal/mol) have been obtained considering acetonitrile as solvent. [b] The reaction product does not correspond to an energy minimum structure and evolves back to reactant (the FeFe complex + triflic acid).

The compound [(dppv)(CO)Fe(edt)Fe(CO)$_3$] (**3**), which differs from **1** for the replacement of the PMe_3 group with a CO ligand, has been experimentally characterized[58] and is similar to another more recently reported synthetic complex ([(dppe)-(CO)Fe(pdt)Fe(CO)$_3$)], which has been shown to undergo μ-protonation at room temperature and terminal-protonation at low temperature (203 K).[66]

The species **3** is less electron-rich than **1**, due to the presence of an extra CO. In fact, the reaction free energy for μ- and terminal protonation is increased by ∼12−14 kcal/mol when compared to **1**. Remarkably, the computed reaction barrier corresponding to μ-protonation of **3** is 3.1 kcal/mol higher than the corresponding value computed for **1**, even though protonation of the Fe−Fe bond in **3** is slightly less affected by steric crowding, due to the smaller size of the CO ligand relative to PMe_3. Therefore, it may be concluded that the decreased reactivity of the Fe−Fe bond in **3** relative to **1** has to be ascribed mainly to electronic factors.

Similarly to what was observed studying **1**, terminal protonation of **3** at Fe_d leads to an isomer that is slightly lower in energy (0.3 kcal/mol) than the most stable isomer obtained from protonation at Fe_p. We were not able to locate the transition state structure for protonation at the terminal position in **3**, since H^+ spontaneously moves back to triflate during optimization.

Reaction energies and barriers computed for the simplified model **4** (Table 1), in which the bulky dppv present in **3** is replaced by two PH_3 ligands (coordinated to the same iron ion), are extremely similar to the corresponding values obtained for **3**, confirming that electronic factors are responsible for the lower reactivity (from both a thermodynamics and kinetics perspective) of species featuring only two phosphine ligands, such as **3** and **4**, with respect to **1**.

Analysis of the complexes **5** and **6**, which are characterized by four symmetrically placed phosphine ligands, reveals other interesting trends. As for reaction thermodynamics, the presence of an extra phosphine ligand (relative to **1**) leads to very exoergonic protonation reactions (Table 1). Formation of μ-protonated isomers is more favored (by ∼3−4 kcal/mol) than terminal protonation. In addition, the energy gap between μ- and terminal-protonated isomers becomes even larger when optimization of the μ- and terminal-H adducts is carried out removing the triflate ion (ΔG between terminal- and μ-protonated isomers = 6.3 and 9.3 kcal/mol for **5** and **6**, respectively), in agreement with experimental studies which showed that terminal-H species derived from **5** and **6** spontaneously isomerize to the corresponding bridging hydrides.[47,49]

As for kinetics effects, the replacement in **1** of a CO and the dppv ligand with three PMe_3 groups (species **5**) causes the reaction barrier for μ-protonation to be almost halved. When two bulky dppv groups (in **6**) replace the four PMe_3 ligands in **5**, the reaction barriers for μ- and terminal-protonation become extremely large (19.6 and 16.6 kcal/mol, respectively), highlighting again the role of steric factors. Analysis of the reaction energy profiles for terminal protonation at Fe_d reveals that the energy barrier does not change significantly when moving from **1** to **5**, whereas Fe_d protonation in **6** is kinetically hindered due to the bulkiness of dppv.

Finally, the reactivity of **7** and **7a** has been compared to evaluate how the energy profile of the protonation reaction is affected by an uneven distribution of phosphine ligands. It turned out that the unsymmetrical coordination environment in **7a** leads to a more exoergonic protonation reaction (compared to **7**), for both μ- and terminal protonation (Table 1). In any case, the μ-H isomer remains the thermodynamically most stable form. When considering reaction barriers, since the presence of very small PH_3 ligands in **7** makes the Fe−Fe bond accessible, μ-protonation becomes more kinetically preferred than terminal protonation. More remarkably, terminal protonation of **7a** is almost barrierless, because rotation of the $Fe_d(CO)_2PH_3$ group is promoted by the electron richness of the Fe_p atom, which is coordinated by three PH_3 units.

Discussion

The high efficiency of dihydrogen production by [FeFe] hydrogenases stems, among several factors, from the protonation regiochemistry of the H-cluster. In fact, initial protonation of the H-cluster might take place in two different ways. Protonation of the Fe−Fe bond of the $[2Fe]_H$ subcluster, leading to μ-H species, or terminal protonation to the five-coordinated distal iron atom. The latter possibility was first proposed by Fontecilla-Camps and collaborators on the basis of X-ray crystallographic results.[23] Both possibilities have been thoroughly investigated by DFT calculations,[67,68] and computational studies eventually converged to a scenario in which only terminal protonation would be associated to kinetically unhindered reaction pathways leading to H_2 formation.[69−71] The higher reactivity of terminal hydride species, when compared to μ-hydride species, was conclusively established by Rauchfuss and co-workers studying synthetic models structurally related to the $[2Fe]_H$ subcluster.[47]

In light of the above considerations, understanding the factors affecting protonation regiochemistry in synthetic models inspired by the $[2Fe]_H$ subcluster is therefore a crucial issue to be addressed for the rational design of efficient synthetic catalysts. With the aim of contributing to shed light on this issue, we have investigated the reaction of a prototypical strong acid (CF_3SO_3H) with a series of diiron compounds differing in the number and nature of phosphine ligands and corresponding to or closely resembling experimentally investigated complexes.

Some broad considerations can be initially pointed out about the thermodynamics and kinetics of the reaction under investigation. Protonation of iron atoms in $[Fe(I)]_2(edt)(PR)_x(CO)_{(6-x)}]$ ($x = 0, 2, 3, 4$) complexes becomes thermodynamically more favorable as the ratio between phosphine and CO ligands increases, as well as when PH_3 ligands are replaced by better electron-donor phosphines, such as PMe_3. This trend is valid for formation of both μ- and terminal-H species and can be simply explained considering that more and better electron-donor ligands increase the electron density on the Fe atoms, which therefore become more basic. More importantly, protonation at the Fe−Fe bond is always thermodynamically favored relative to terminal iron protonation, irrespective of the ligand stereoelectronic properties.

The electron donor properties of the ligands affect also reaction barriers ($\Delta G^{\ddagger}$). In general, with the exception of dppv complexes, in which steric factors become more important, the presence of phosphines, which are better electron donors than CO ligands, leads to smaller barriers.

More subtle observations regarding protonation regiochemistry can be derived by the comparative analysis of the reactivity of model complexes **1**−**7**. In this context, it is worth reminding that one of the major and more puzzling experimental differences observed when studying unsymmetrical $[Fe_2(CO)_4(\kappa_2\text{-LL})(pdt)]$ and symmetrical $[Fe_2(CO)_4(L)_2(pdt)]$ species lies in protonation regiochemistry. In fact, using the same experimental conditions, it was observed that while $[Fe_2(CO)_4(PMe_3)_2(pdt)]$ and $[Fe_2(CO)_4(P(OMe)_3)_2(pdt)]$ give exclusively μ-hydride species upon protonation,[35] intermediates featuring a terminal-hydride could be detected at low temperature investigating $[Fe_2(CO)_4(\kappa_2\text{-LL})(pdt)]$ complexes.[35,44−46,66] In light of these results, it was suggested that the unsymmetrical arrangement of the ligands could be a key factor for the formation of terminal-hydride species.

The DFT investigation of the asymmetric models included in our set (**1**, **3**, **4**, and **7a**) shows that, from a thermodynamics perspective, protonation generally takes place preferentially on the less electron-rich iron atom, i.e., the iron atom coordinated by the largest number of CO ligands. This trend is consistent with experimental data[43] and can be explained as follows. On the one hand, protonation of the Fe atom coordinated by the largest number of phosphine ligands is favored because this iron atom is the electron richest but disfavored because in the reaction

(54) Bertini, L.; Bruschi, M.; de Gioia, L.; Fantucci, P.; Greco, C.; Zampella, G. *Atomistic Approaches in Modern Biology: From Quantum Chemistry to Molecular Simulations*; Springer: Berlin, New York, 2007; Vol. 268, pp 1−46.
(55) Bruschi, M.; Zampella, G.; Fantucci, P.; De Gioia, L. *Coord. Chem. Rev.* **2005**, *249*, 1620–1640.
(56) Bruschi, M.; Greco, C.; Zampella, G.; Ryde, U.; Pickett, C. J.; De Gioia, L. *C. R. Chim.* **2008**, *11*, 834–841.
(57) Schafer, A.; Klamt, A.; Sattel, D.; Lohrenz, J. C. W.; Eckert, F. *Phys. Chem. Chem. Phys.* **2000**, *2*, 2187–2193.
(58) Justice, A. K.; Zampella, G.; De Gioia, L.; Rauchfuss, T. B.; van der Vlugt, J. I.; Wilson, S. R. *Inorg. Chem.* **2007**, *46*, 1655–1664.
(59) Eilers, G.; Schwartz, L.; Stein, M.; Zampella, G.; de Gioia, L.; Ott, S.; Lomoth, R. *Chem.—Eur. J.* **2007**, *13*, 7075–7084.
(60) Wang, F. J.; Wang, M.; Liu, X. Y.; Jin, K.; Donga, W. B.; Sun, L. C. *Dalton Trans.* **2007**, 3812–3819.
(61) Schwartz, L.; Eilers, G.; Eriksson, L.; Gogoll, A.; Lomoth, R.; Ott, S. *Chem. Commun.* **2006**, 520–522.
(62) Gao, W. M.; Ekstrom, J.; Liu, J. H.; Chen, C. N.; Eriksson, L.; Weng, L. H.; Akermark, B.; Sun, L. H. *Inorg. Chem.* **2007**, *46*, 1981–1991.
(63) Singleton, M. L.; Jenkins, R. M.; Klernashevich, C. L.; Darensbourg, M. Y. *C. R. Chim.* **2008**, *11*, 861–874.
(64) Thomas, C. M.; Darensbourg, M. Y.; Hall, M. B. *J. Inorg. Biochem.* **2007**, *101*, 1752–1757.
(65) Tye, J. W.; Darensbourg, M. Y.; Hall, M. B. *Inorg. Chem.* **2006**, *45*, 1552–1559.
(66) Ezzaher, S.; Capon, J. F.; Gloaguen, F.; Petillon, F. Y.; Schollhammer, P.; Talarmin, J. *Inorg. Chem.* **2007**, *46*, 3426–3428.
(67) Fan, H. J.; Hall, M. B. *J. Am. Chem. Soc.* **2001**, *123*, 3828–3829.
(68) Zampella, G.; Greco, C.; Fantucci, P.; De Gioia, L. *Inorg. Chem.* **2006**, *45*, 4109–4118.
(69) Siegbahn, P. E. M.; Tye, J. W.; Hall, M. B. *Chem. Rev.* **2007**, *107*, 4414–4435.
(70) Bruschi, M.; Greco, C.; Fantucci, P.; De Gioia, L. *Inorg. Chem.* **2008**, *47*, 6056–6071.
(71) Greco, C.; Bruschi, M.; De Gioia, L.; Ryde, U. *Inorg. Chem.* **2007**, *46*, 5911–5921.

Scheme 5. Competition between Different Protonation Pathways in Asymmetric FeFe Complexes

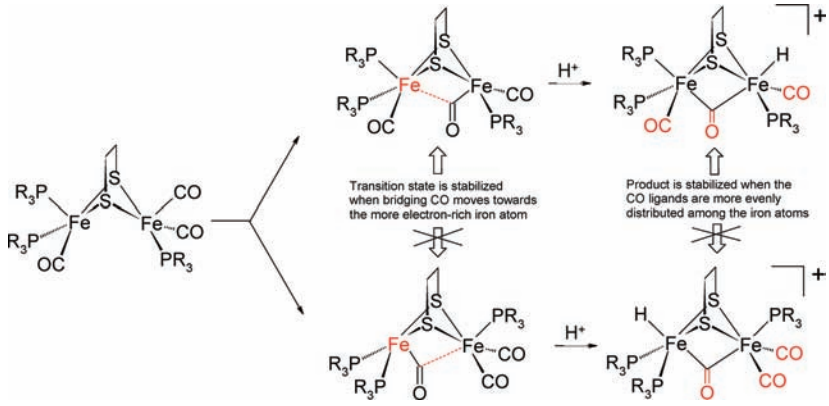

product the CO ligands (which compete among themselves for back-donation from the iron atoms) are all coordinated to the same metal center (Scheme 5). On the other hand, protonation on the iron atom coordinated by a few (or none) phosphines is disfavored because it is less electron-rich. However, in the reaction product the CO ligands are more symmetrically distributed, decreasing the competition for back-donation. The two effects are almost balanced when very small phosphorus-containing ligands (such as PH_3; data not shown) are present. However, when the phosphine ligand coordinated to Fe_p is dppv, also steric factors play a role, and therefore preferential protonation at the less electron-rich iron atom is observed. In addition, it is also worth noting that protonation of Fe_d is more favored in $[(CO)(PR_3)_2Fe_p(edt)Fe_d(CO)_2(PR_3)]$ than in the more asymmetrical $[(CO)(PR_3)_2Fe_p(edt)Fe_d(CO)_3]$ species, highlighting the importance of the presence of *at least one* electron-donor ligand coordinated to Fe_d to allow thermodynamically facile terminal protonation. The latter observation nicely agrees with the recent report showing that in the synthetic complex $[(CO)(dppe)Fe_p(\mu\text{-}SCH_2N(^iPr)CH_2S)Fe_d(CO)_3]$ protonation takes place exclusively at the N atom, and proton transfer from the protonated chelating ligand to Fe_d is not spontaneous.[72] In light of these results, it can be speculated that one of the reasons for the presence of a CN^- ligand coordinated to Fe_d in the enzyme might be related to the facile formation of catalytically relevant terminally protonated species.

In asymmetric species, terminal protonation takes place preferentially at the less electron-rich Fe atom also from a kinetic perspective. In fact, terminal protonation implies the transit through a transition state in which two of the ligands of the protonating Fe ion rotate, bringing one CO ligand into a semibridging position (Figure 2). As also discussed in previous studies,[65] the formation of the μ-CO transition state is favored by back-donation from the "nonrotating" Fe atom to the μ-CO group. Therefore, in diiron complexes featuring an asymmetric distribution of phosphine ligands, terminal protonation is kinetically preferred at the less electron-rich iron atom (Scheme 5).

It must be noted that the uneven distribution of phosphine ligands cannot be the only key requisite for the formation of terminal hydrides in synthetic complexes, since the formation of transient terminal-hydride species (which eventually convert to μ-hydride forms) has been observed also in studying the protonation of symmetric complexes, such as $[Fe_2(CO)_2(dppv)_2(pdt)]$ (which correspond to model **6**).[47] Our results obtained investigating the set of complexes **1**−**7** highlight how the presence of bulky phosphine ligands, which severely hinder the accessibility to the Fe−Fe bond, is a crucial factor responsible for the kinetic preference of terminal versus μ-protonation in symmetric complexes. In fact, μ-protonation is characterized by a lower energy barrier than terminal protonation only in the case of a symmetric complex characterized by sterically undemanding PH_3 ligands (complex **7**).

The importance of steric effects in the kinetics of protonation of diiron complexes containing bulky ligands is well highlighted by the large $\Delta G^{\ddagger}$ values computed investigating complex **6** ($\Delta G^{\ddagger}$ > 16 kcal/mol), showing that both terminal and μ-protonation are affected, even if to a different extent, by the dppv bulkiness. In this context, DFT results may also contribute to the interpretation of recent results obtained by Rauchfuss and co-workers, which showed that $[Fe_2(pdt)(CO)_2(dppv)_2]$ and $[Fe_2(adt)(CO)_2(dppv)_2]$ are characterized by a very different reactivity with acids.[73] In particular, it was found that the thermodynamic stability of the terminal-hydride species formed upon reaction of $[Fe_2(pdt)(CO)_2(dppv)_2]$ and $[Fe_2(adt)(CO)_2(dppv)_2]$ with suitable acids is comparable, whereas the kinetics of formation is very different, with $[Fe_2(adt)(CO)_2(dppv)_2]$ reacting much faster than $[Fe_2(pdt)(CO)_2(dppv)_2]$. In light of our results showing that the presence of dppv makes both μ- and terminal protonation kinetically difficult, due to the inaccessibility of the iron atoms, it can be proposed that terminal protonation of $[Fe_2(adt)(CO)_2(dppv)_2]$ is faster than that for $[Fe_2(pdt)(CO)_2(dppv)_2]$ because the proton is initially (and quickly) transferred to the NH group of the chelating ligand, which is sterically unhindered. Then, subsequent intramolecular proton transfer from protonated adt to iron, leading to a terminal hydride, is facile because the acid ($adtH^+$) is already embedded within the molecule structure (i.e., not affected by dppv bulkiness) and in proximity of one of the iron atoms.

In conclusion, the DFT investigation of the reaction between a strong acid and a series of $[Fe(I)]_2(edt)(PR)_x(CO)_{(6-x)}]$ ($x = 0, 2, 3, 4$) models has allowed us to rationalize the role of electronic and steric factors for protonation regiochemistry, from both a kinetics and thermodynamics perspective. These results might also give some hints for the rational design of efficient synthetic catalysts. As recently noted by Darensbourg and collaborators,[27] the synthesis of efficient synthetic catalysts maintaining the μ-CO "rotated"

(72) Ezzaher, S.; Orain, P. Y.; Capon, J. F.; Gloaguen, F.; Petillon, F. Y.; Roisnel, T.; Schollhammer, P.; Talarmin, J. *Chem. Commun. (Camb)* **2008**, 2547–9.

(73) Barton, B. E.; Olsen, M. T.; Rauchfuss, T. B. *J. Am. Chem. Soc.* **2008**, *130*, 16834–5.

structure throughout all the redox process leading to dihydrogen production is a formidable challenge. Experimental and computational results have shown that the formation of catalytically competent terminal-hydride species can be favored also when the Fe(I)Fe(I) precursor does not feature a μ-CO ligand, if the iron ligands have the proper stereoelectronic features. However, poorly reacting μ-H Fe(II)Fe(II) species are always thermodynamically more stable than the corresponding terminal-hydride forms. How to "freeze" the spontaneous isomerization from terminal- to μ-H species in synthetic models of [FeFe] hydrogenases is still an open challenge.

Acknowledgment. We thank Prof. T. B. Rauchfuss for insightful discussions.

Supporting Information Available: Absolute energies and optimized geometries of all calculated structures, figures of the lowest energy structures obtained by protonation of **1**, van der Waals representation of **1a**, and comparison between DFT and X-ray structures for selected complexes. This material is available free of charge via the Internet at http://pubs.acs.org.

JA902727Z